Toward a Rational Design of Peptide Inhibitors of Ribonucleotide Reductase: Structure−Function and Modeling Studies

Bari A. Pender,[‡] Xu Wu,[‡] Paul H. Axelsen,[§] and Barry S. Cooperman*[,‡]

Departments of Chemistry and Pharmacology, University of Pennsylvania, Chemistry Building, Philadelphia, Pennsylvania 19104

Received August 3, 2000

Mammalian ribonucleotide reductase, a chemotherapeutic target, has two subunits, mR1 and mR2, and is inhibited by AcF[1]TLDADF[7], denoted P7. P7 corresponds to the C-terminus of mR2 and competes with mR2 for binding to mR1. We report results of a structure−function analysis of P7, obtained using a new assay measuring peptide ligand binding to mR1, that demonstrate stringent specificity for Phe at F^7, high specificity for Phe at F^1, and little specificity for the N-acyl group. They support a structural model in which the dominant interactions of P7 occur at two mR1 sites, the F^1 and F^7 subsites. The model is constructed from the structure of *Escherichia coli* R1 (eR1) complexed with the C-terminal peptide from eR2, aligned sequences of mR1 and eR1, and the trNOE-derived structure of mR1-bound P7. Comparison of this model with similar models constructed for mR1 complexed with other inhibitory ligands indicates that increased F^1 subsite interaction can offset lower F^7 subsite interaction and suggests strategies for the design of new, higher affinity inhibitors.

I. Introduction

Ribonucleotide reductase (RR) catalyzes the reduction of ribonucleotides to 2′-deoxyribonucleotides, the rate-limiting step of DNA biosynthesis. Class I RRs, which include RR from eucaryotes, *Escherichia coli*, and certain bacteriophages and viruses, are composed of two subunits, R1 and R2. R1 contains the active site as well as binding sites for allosteric ligands, while R2 contains a μ-oxo bridged diferric center, which is required for generating, and presumably stabilizing, a catalytically essential tyrosine radical. Enzyme activity is initiated via electron transfer between the active site in R1 and the conserved tyrosine radical in R2, and it is completely dependent on the association of the two subunits.[1,2]

RR has been shown to be linked with malignant transformation and tumor cell proliferation[3] and is a well-recognized target for cancer chemotherapeutic and antiviral agents.[3,4] The RR inhibitors hydroxyurea and 2′-deoxy-2′,2′-difluorocytidine (gemcitabine) are used in clinical practice to treat certain types of leukemia[3] and pancreatic cancer,[5] respectively. Clinical trials are underway to broaden the use of these compounds, sometimes in combination with others, for both cancer and HIV chemotherapy.[6−13] Because both compounds have toxic side effects,[6,14−16] and it is clear that resistance to RR inhibitors may emerge during therapy,[17] the development of safer, more efficacious ribonucleotide reductase inhibitors remains a high priority for RR-targeted chemotherapies.

Inhibitors that disrupt enzyme quaternary structure remains an attractive goal, because of the intrinsically higher specificity offered by this approach.[18] We have demonstrated previously that the N-acetylated peptide AcF[1]TLDADF[7], denoted P7, which corresponds to the seven C-terminal residues of mouse R2 (mR2), binds to mouse R1 (mR1), blocking subunit association and inhibiting enzyme activity.[19] Our choice of P7 was based on the strong homology among eucaryotes and some viruses for the seven residues at the C-terminus of eucaryotic R2, a homology that has been reinforced by new additions to the sequence database (Table 1). Subsequent structure−function studies[20] resulted in the following conclusions: (1) P7 is the minimal core peptide length required; deletions result in loss of inhibitory activity, while extensions at the N-terminus have little effect. (2) A free carboxylate is required at the C-terminus. (3) Positions 1 and 7 have a strong preference for Phe, as seen by a >40-fold loss of activity on Leu substitution. (4) The charged/polar residues at positions 2 and 6 are not crucial to peptide binding, although these residues are evolutionarily conserved in mammalian R2 C-termini.[20] As demonstrated by trNOE NMR,[21,22] the mR1-bound structures of both P7 and AcYTLDADF have reverse turn conformations. On the basis of these structures, we have designed and synthesized two new sets of compounds: (1) cyclic lactam peptides, one of which (AcFcyc[ELDK]DF, denoted cycP7) is a 2.5-fold more potent inhibitor of mRR than P7,[23,24] and (2) a tetrahydropyran-based β-turn mimetic which was less successful.[25]

Our efforts continue to focus on generating more potent inhibitors of mRR. Below we describe the synthesis of three positional libraries derived from P7, of general structures AcFTLDADX, AcXTLDADF, and XC(O)FTLDADF. These libraries are tested using a new assay that measures the ability of a given potential ligand to compete with Sepharose-FTLDADF binding to mR1, giving results equivalent to effects on mRR activity. These and other structure−function results are rationalized in terms of a structural model of the

* To whom to address correspondence. Tel: (215) 898-6330. Fax: (215) 898-2037. E-mail: cooprman@pobox.upenn.edu.
‡ Department of Chemistry.
§ Department of Pharmacology.

10.1021/jm000335r CCC: $20.00
Published on Web 12/08/2000

Table 1. Comparison of Seven C-Terminal Residues of R2 and Residues 339, 340, 343, 725, 728, and 729 (mR1 numbering) at the R1 Peptide Binding Site[a]

ORGANISM	mR1 residue #						R2 C-Terminus
	339	340	343	725	728	729	
HSV type 1/strain 17	F	K	I	V	Y	K	GAVVNDL
HSV type 2/strain 333	F	K	I	V	Y	K	GAVVNDL
Herpesvirus saimiri/strain 11	F	K	E	L	F	R	GTLTNDL
Epstein-barr virus/strain B95-8	F	K	R	T	Y	E	MLVVDDL
Bovine HSV type 1/strain Cooper	F	D	L	V	Y	K	GTVINDL
Pseudorabies Virus/strain Kaplan	F	Q	Q	M	Y	N	GTVVNDL
Equine HSV type 1/subtype 2	F	D	Q	V	Y	K	GTLINDL
Equine HSV type 1/strain Ab4p	F	D	Q	V	Y	K	GTLINDL
Varicella-zoster virus/strain Dumas	F	E	L	I	Y	K	GTVINDL
E. coli	Y	T	L	L	Y	K	DLSNFQL
Salmonella typhimurim	Y	T	L	L	Y	K	DLSNFQL
H. influenzae	Y	Q	I	L	Y	K	DFDDFSL
Human	M	K	E	F	W	K	FTLDADF
Mouse	M	K	E	F	W	K	FTLDADF
Brachydanio rerio (Zebrafish)	M	K	E	F	W	K	FTLDADF
Vaccinia Virus/strain Copenhagen	M	K	K	F	W	S	FSLDVDF
Vaccinia Virus/strain WR	M	K	K	F	W	S	FSLDVDF
Variola Virus	M	K	K	F	W	S	FSLDVDF
C. elegans	M	K	E	F	W	K	FDLEADF
S. pombe (fission yeast)	M	Q	E	F	W	K	FTIDEDF
S. cerevisiae (bakers yeast)	M	K	E	F	W	K	FTFNEDF
Plasmodium falciparum/isolate Dd2	M	K	K	F	W	E	FCLNTEF
Plasmodium falciparum/FCR-3/Gambia	M	K	K	F	W	E	FCLNTEF
Trypanosoma brucei brucei	M	E	E	F	W	K	FSLDADF
Bacteriophage T4	M	E	G	L	W	Y	MSFKKYF
African swine fever virus/strain BA71V	M	E	E	V	W	K	LFLNDDF
African swine fever virus/isolate Malawi Lil 20/1	M	E	E	V	W	K	LFLDDDF
Mycoplasma genitalium	F	Q	K	I	F	K	NDDDWNF
Mycoplasma pneumoniae	F	T	K	I	F	K	EDKDWDF
Mycoplasma tuberculosis	F	E	K	I	W	R	TDTDWDF
Helicobacter pylori	L	K	L	T	W	K	SVSFDDF
Treponema pallidum	W	K	R	V	W	E	SAMVDDL
Bacillus subtilis	V	E	R	L	H	H	EDEKEQI

[a] Sequences were downloaded from the protein sequence database (EMBL, Switzerland). The binding site alignment is based on the observed peptide binding site in the *E. coli* crystal structure[26] and multiple sequence alignments made using CLUSTALW at the Institute for Biomedical Computing, Washington University of St. Louis, St. Louis, MO.

mR1.P7 complex that is based on the crystal structure of the R1 from *E. coli* (eR1) complexed with the C-terminal peptide from *E. coli* R2 (eR2),[26] the aligned sequences of mR1 and eR1, and the trNOE-derived structure of P7 bound to mR1. A similar approach is used to model the structure of cycP7 bound to mR1. The combination of the structure−function and modeling results provides specific suggestions for the development of new, high affinity inhibitors of mRR.

II. Results and Discussion

A New mR1-Peptide Binding Assay. In earlier work we evaluated the efficacy of peptide inhibitors in an in vitro RR activity assay, which yields a K_i value (in the form of an IC_{50}) for a given inhibitor.[19,20] However, this assay, which is based on a column separation of product from substrate, is cumbersome for screening a large number of compounds, and requires materials that are both costly and radioactive.

Here we introduce a new, simpler assay that measures the direct competition between an inhibitory ligand and P7 for the peptide-binding site on the mR1 protein, eliminating the need for both mR2 protein and radioactive substrate. The assay is based on an application of the FTLDADF-Sepharose affinity column introduced earlier for mR1 purification.[19] It measures the amount of mR1 eluted when a mixture of mR1 and the candidate inhibitor are drawn through the affinity column by centrifugation. The higher the affinity of an inhibitory ligand for mR1, the more mR1 is eluted. Comparison of the results obtained with P7 allows a quantitative estimate of the K_d of the candidate inhibitory ligand (see Experimental Section). The close agreement in the results obtained for several potential inhibitory ligands in both the activity and binding assays (Table 2) validates the new assay. Importantly, the new assay directly tests that the candidate molecule is inhibiting enzyme activity by binding to the R2 C-terminal peptide site, rather than by another mechanism. This will be especially important for the testing of smaller, less peptide-like inhibitors that should result from the more detailed understanding of the peptide binding site reported in this work (see below).

Structure−Function Studies. The strong conservation of F^1 and F^7 in the C-terminal sequences of eucaryotic R2 (Table 1) suggests that these residues may have strong interactions with mR1, at loci denoted the F^1 and F^7 subsites, respectively, and raises the question of whether gains in affinity toward mR1 could be achieved by substitution at these positions in P7. Further, acetylation of the terminal N is known to be important for P7 binding, but is unclear whether acylation with another group would not confer higher affinity. These points are addressed with the three single position libraries described below, the results for which are summarized in Table 2. These results also led to a preliminary investigation of the binding of simple N-protected derivatives of Phe and Leu.

(a) Library I. AcFTLDADX. Results for library I, including peptides **2**−**25**, lead to the following conclusions regarding the F^7 subsite, and the properties a residue must have for optimal binding to the F^7 subsite.

First, the substituted residue must be aromatic. This is shown by the poor binding of the Cha-substituted peptide, **3**, a result extending the earlier observation that Leu substitution lowers inhibitory activity >40-fold.[20] The Gln-substituted peptide **4** also binds poorly, so that any possible increases in affinity due to H-bonding do not outweigh the loss in affinity on substitution with a nonaromatic residue. Moreover, the precise electronic character of the aromatic ring is apparently critical, judging by the decreases in binding activity when the isosteric[27] fluoro-phenyl or pyridyl groups (peptides **5**−**8**) substitute for phenyl. Thus, a small drop is seen for the *o*-F substitution, while decreases on F_5-Phe or pyridyl substitution are much larger.

Second, the size and placement of the aromatic residue are crucial, as shown by the poor binding activities of the peptides substituted either with the other coded aromatic amino acids, Tyr, Trp, and His (**9**−**11**), or with Phg (**12**). Elsewhere[28] it has been reported that homoPhe substitution at position lowers affinity only 2-fold, so that the F^7 subsite appears less sensitive to overfilling than to underfilling (**12**). Interestingly, substitution with the D-Phe isomer (**13**) results in only a relatively small decrease in binding affinity (7-fold). This substitution may distort the peptide in a manner similar to the cyclic peptide cycP7, though with a less favorable effect on binding, as discussed below.

Third, we note a large loss in binding activity on replacing the carboxylate with carboxamide (**14**), implicating the need for a negative charge at the C-terminus. Consistent with this conclusion is the earlier finding of a 50-fold drop in inhibitory potency for the peptide AcFTLDADFAA (**15**),[20] which extends P7 at the C-terminus.

Fourth, the F7 subsite is very constrained sterically, since ring substitution at the *o*-, *m*-, and *p*-positions of a C-terminal Phe all lead to lower binding (**16**−**25**). The amino, hydroxy-, and methoxy-substituted derivatives were designed as possible hydrogen bond donors and acceptors. Clearly, any possible positive effect of such substitution is more than outweighed by negative steric and/or other factors.

Fifth, the F7 subsite has a hydrophobic character, as demonstrated most clearly by the correlation between hydrophobicity and affinity for the six peptides with *p*-substitution in the C-terminal Phe. Thus, the two substituents with positive Π values (Table 3a), *p*-CH_3 and *p*-Cl (**22**, **23**), confer much smaller losses in affinity (3−4-fold reductions), the *p*-OCH_3 (**24**) derivative which has a Π value close to zero confers an intermediate loss (16-fold worse), whereas the four substituents with negative Π values, *p*-OH (**9**), *p*-NH_2 (**25**), and *p*-NO_2 (**19**, which is 47% of the *o*-OMe:*p*-NO_2 mixture, see Experimental section) exhibit dramatic losses in binding affinity (≥20-fold reductions). In addition, the affinities of peptides with coded aromatic amino acids in the C-terminal position also correlate with their relative hydrophobicities: Phe (**1**) > Trp (**10**) > Tyr (**9**), His (**11**) > Gln (**4**) (Table 3b).

Summing up, all substitutions for Phe at the C-terminus of P7 lead to decreased binding activity. The very stringent binding requirements that can be inferred from these results make it unlikely that peptide binding affinity can be increased through substitution at the C-terminus, at least for linear peptides.

(b) Libraries II, AcXTLDADF, and III, XC(O)-

Table 2. Relative Binding Affinities of Peptide Inhibitors of Mouse RR

Substitution vs. P7	RR inhibitor, #	Relative K_d[a]	Relative K_i[b]
none	P7, **1**	(1.0)	(1.0)
At residue #7 (Library I)	Leu, **2**		> 35[c]
	Cha, **3**	12 ± 1	
	Gln, **4**	> 30	
	o-F, **5**	2.0 ± 0.1	
	F_5-Phe, **6**	16 ± 1	
	2-Pyr, **7**	21 ± 5	
	3-Pyr, **8**	> 30	
	Tyr, **9**	24 ± 1	
	Trp, **10**	10 ± 2	
	His, **11**	29 ± 3	> 20
	Phg, **12**	24 ± 3	
	D-Phe, **13**	8.6 ± 0.1	
	Phe-NH_2, **14**	> 30	
	PheAlaAla, **15**		> 35[c]
	o-OH-Phe, **16**	26 ± 1	
	o-Cl-Phe, **17**	12 ± 1	
	o-OCH_3-Phe, **18**/ p-NO_2-Phe, **19**[d]	> 30	
	m-OH-Phe, **20**	6.3 ± 0.7	
	m-OCH_3-Phe, **21**	8.2 ± 0.5	
	p-Cl-Phe, **22**	3.1 ± 0.1	3.2 ±0.5
	p-CH_3-Phe, **23**	4.7 ± 0.1	
	p-OCH_3-Phe, **24**	16 ± 4	
	p-NH_2-Phe, **25**	23 ± 3	
At residue #1 (Library II)	Cha, **26**	> 30	
	Leu, **27**	> 30	
	Val, **28**	> 30	
	Ala, **29**	> 30	
	Tyr, **30**		15[e]
	Phg, **31**	6.6 ± 0.1	
	2-Nal, **32**	2.1 ± 0.5	
	Desamino-Phe, **33**		> 40[f]
Terminal N-acylation (library III)	None, **34**		> 40[g]
	4,4'-dicarboxy-2,2'-bipyridyl-, **35**	0.6 ± 0.1	
	p-NO_2-phenyl acetyl-, **36**	0.8 ± 0.1	
	phenyl acetyl-, **37**	0.8 ± 0.1	
	p-OCH_3- phenyl acetyl-, **38**	0.8 ± 0.1	
	Butanoyl-, **39**	1.0 ± 0.1	
	Benzoyl-, **40**	1.9 ± 0.7	
	Fmoc-, **41**	1.4 ± 0.1	
	Formyl, **42**	2.4 ± 0.4	
	Propionyl, **43**	6.3 ± 0.1	
N-protected amino acids	FmocPhe	13 ± 1	17 ± 1
	FmocLeu		~ 17
	Boc-Phe		>80

[a] New binding assay. [b] Activity assay. [c] Reference 20. [d] Assayed as a 53:47 **18**:**19** mixture. [e] Reference 21. [f] S. Nair, private communication. [g] Reference 19.

Table 3. Measures of Hydrophobicity

(a) Comparison of the Hydrophobic Character of Substituents on an Aromatic Ring (Π)[50]

substituent	Π value[a]
pCl	+0.71
pCH_3	+0.56
$pOCH_3$	−0.02
pNO_2	−0.28
pOH	−0.67
pNH_2	−1.23

(b) Comparison of the Hydrophobicities of the Coded Amino Acids[51]

amino acid	hydrophobicity[b] (kcal/mol)
Leu	−3.98
Phe	−2.04
Trp	−1.39
Tyr	+1.08
His	+5.60
Gln	+6.48

[a] Reference 50. [b] Reference 51.

FTLDADF. Library II probes the importance of the N-terminal Phe. The results obtained (Table 2) parallel those obtained with library I in indicating the importance of an aromatic residue at this position, as each of the substitutions containing an aliphatic side chain, including Cha (**26**) and Leu (**27**), had quite reduced binding activity (>30-fold). By contrast, each of the substitutions containing an aromatic side chain had measurable binding activity, albeit lower than P7 itself, and the effects of identical substitutions [Tyr (**30**), Phg (**31**)] were less deleterious at position 1 than at position 7. We interpret these results as suggesting a lower binding stringency at the F^1 subsite than at the F^7 subsite, raising the possibility that affinity might yet be increased through suitable substitution at this site, e.g., substituted naphthyl (**32**) derivatives.

Library III probes the importance of the nature of the acyl group capping the terminal nitrogen. Evidence that the amide formed by N-terminal acylation contributes to peptide affinity, rather than simply removing the negative effect of a positively charged ammonium group, is provided by the result that the desamino derivative (**33**) has very poor inhibitory activity. However, the positive effect seems to be confined to the amide group itself, and is largely independent of the nature of carbamide substitution. Minor enhancement in binding activity is obtained with large aromatic acyl groups (**35**−**38**), but the effects are less than 2-fold vis-à-vis P7, and even a formyl capping group (**42**) affords a peptide having an affinity only 2-fold less than P7 itself. These results suggest that the group attached to the carbonyl has little interaction with mR1, consistent with our earlier finding that the acetylated forms of the mR2 C-terminal octamer and nonamer have the same inhibitory activity as P7.[20]

(c) N-Protected Phe and Leu. The clear indication of strong interactions at the F^7 and F^1 subsites led us to investigate N-terminally protected Phes as ligands for mR1, as assayed via inhibition of mRR activity, because of the greater dynamic range of this assay. Interestingly, FmocPhe inhibited mRR with an apparent K_i only 17-fold higher than P7. Moreover, such inhibition arises from competitive binding to mR1, since the activity of FmocPhe in the binding assay (13-fold weaker than P7) was virtually identical. By contrast, Boc-Phe showed very much poorer inhibition of mRR activity (≥100-fold weaker than P7), indicating that FmocPhe is interacting primarily via the Fmoc group rather than via Phe. This suggestion is supported by the finding that FmocLeu inhibited mRR equally as well as FmocPhe. The important implications of relatively strong FmocPhe and FmocLeu binding are considered further below.

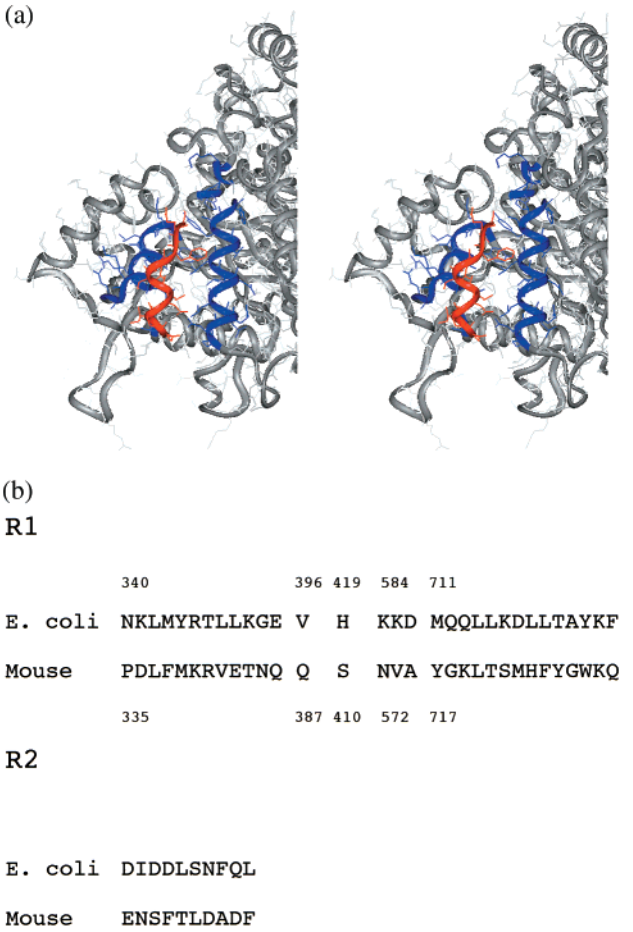

Figure 1. *E. coli* R1 peptide binding site. (a) Stereoview of the peptide binding site in the eR1 crystal structure with bound eR2 peptide (pdb reference code 1RlR). Colored in red is the eR2 peptide. Colored in blue are the residues within 7 Å of the peptide, including the αI and α13 helicies. (b) CLUSTALW alignment of mR1 residues with eR1 residues 7 Å from the eR2 peptide.

Models of P7 and cycP7 Bound to mR1. Three-dimensional models of P7 and cycP7 bound to mR1 were constructed, based on (a) the known crystal structure of the complex between eR1 and 10 C-terminal residues of bound eR2 C-terminal peptide[26] (the structure of mR1 is unavailable); (b) the aligned primary structures of eR1 and mR1 (Figure 1)—a direct comparison of the eR1 and mR1 sequences showed them to be 29% identical and 53% homologous,[29] constituting compelling evidence for similar three-dimensional structures;[30] and (c) structures of the mR1-bound forms of P7[21,22] and cycP7[23] determined by trNOE. The success of these models in rationalizing the structure−function results summarized in Table 2 and related earlier results, as described below, provides a basis for confidence that they will be useful in guiding the future design of P7 analogues with heightened binding activity toward mR1. Below we use

mR1 numbering throughout in discussing the roles of specific residues.

In the *E. coli* enzyme, the 10 eR2 C-terminal residues bind into a shallow cleft between the antiparallel α-helices 13 (residues 335−345) and I (residues 718−732) in eR1 (Figure 1). Three major lines of evidence suggest especially strong conservation of this interface region. First, biochemical and genetic results show that residues in mR1 and a viral R1 involved in R2 C-terminal peptide binding align with helix αI in eR1. Thus, an azidophenyl derivative of FTLDADF was found to photoincorporate into the 724−735 peptide of mR1,[31] and HSV-R1 variants at positions 1090 and 1091, corresponding to mR1 residues 716 and 717, have been isolated from strains of HSV-1 that show weak resistance to an R2 C-terminal peptidomimetic inhibitor.[32] In addition, the αI sequence partially overlaps a highly conserved R1 sequence (residues 731−738) that includes the functionally important Tyr^{737} and Tyr^{738} residues.[33]

Second, in the eR1 crystal structure, eR1 residues Tyr^{339} in helix α13 and Tyr^{728} in helix αI form a strongly interacting binding pocket for the C-terminal Leu of the bound eR2 peptide. Inspection of a multiple sequence alignment reveals a conserved covariance of these three residues (Table 1). Specifically, for virtually all R2 sequences ending in Leu (procaryotes and some viruses) residues 339 and 728 are always Phe or Tyr, whereas for virtually all R2 sequences ending in Phe (eucaryotes, including mR2, and other viruses) residues 339 and 728 are always Met and Trp, respectively. Since the sum of the side chain volumes of two Phe residues and one Leu residue is almost exactly equal to the sum of the volumes of one Phe, one Trp, and one Met residue,[34] R1 residues 339 and 728 and the C-terminal residue of R2 appear to constitute a conserved hydrophobic cluster of constrained volume at the R1:R2 interface.

Third, mR1-bound P7 has a distinct reverse turn conformation. Residues TLDA comprise this turn, and their 12 backbone heavy atoms can be overlayed with the corresponding atoms of residues LSNF of the bound *E. coli* R2 C-terminal peptide (DIDDLSNFQL) bound to eR1 with an RMSD of 0.35 ± 0.02 Å.[21,22]

Along with these similarities, there is also an important difference between R2 C-terminal binding to eR1 vs mR1. P7 binds to mR1 with a binding affinity of 10 μM and appears to contain virtually the entire binding determinant for mR2 interaction with mR1.[20,35] In contrast, the eR2 C-terminal octamer binds only poorly to eR1 (K_i of 370 μM), and it requires the 20-mer C-terminal peptide to achieve a dissociation constant of 20 μM.[36] This difference suggests that there are contacts between P7 and mR1 that are either not made between eR1 and the eR2 C-terminal octamer or are much weaker. On the basis of the strong sensitivity of P7 binding to mR1 to substitution at both the F^1 and F^7 positions, we believe it likely that the relatively high affinity seen for P7 binding to mR1 reflects significant mR1 interaction with both the C-terminal and N-terminal halves of P7. This contrasts with the eR2 C-terminal octamer ($D^*D^1LSNFQL^7$, numbered so as to be comparable to P7) interaction with eR1, which, as is clear from examination of the eR1-R2 C-terminal structure (pdb 1rlr; see also ref 26), occurs principally via contacts to F^5 and L^7. Noteworthy in this connection is

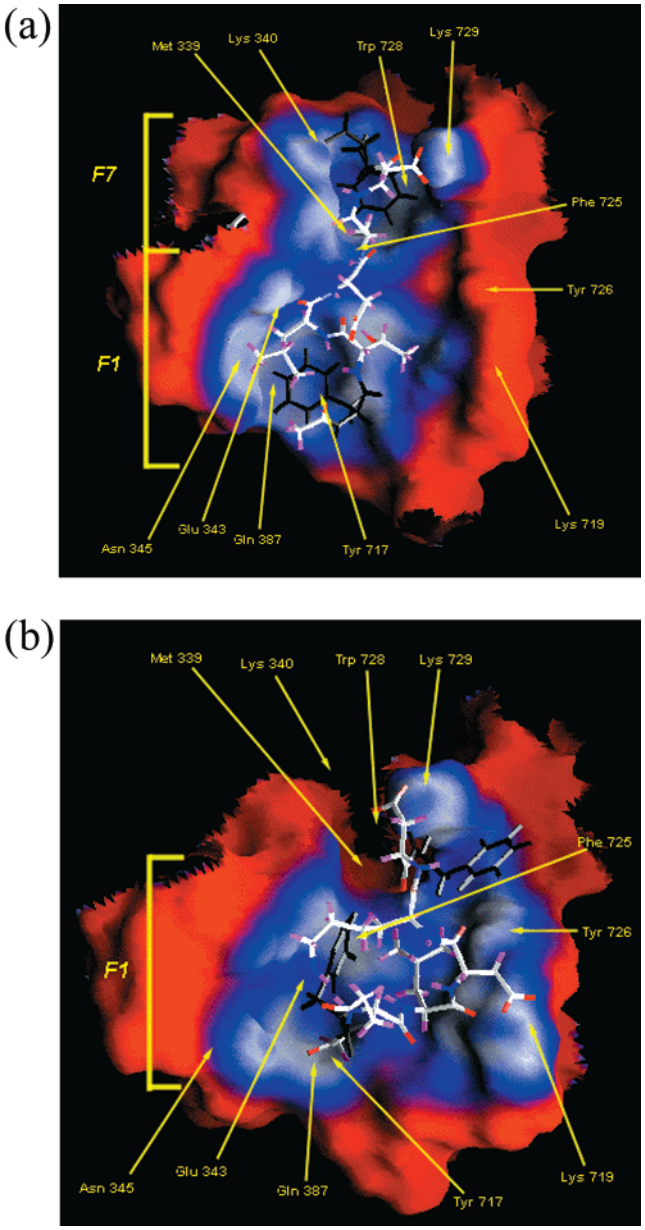

Figure 2. Homology models of mR1 bound with (a) P7; (b) cycP7. Images were generated using GRASP.[52] The binding surface is color coded by distance, with red areas of the model having essentially no contact with the peptide (3 Å from nearest point), blue areas having intermediate contacts (2−3 Å), and white areas having close contacts (1−2 Å). Residues F^1 and F^7 are colored in black. The extent of the F^1 and F^7 subsites, as well as selected residues important for peptide binding (see text for discussion), are indicated in yellow. Especially noteworthy in contrasting panels a and b are the enlarged interaction surface at the F^1 subsite in panel b, which now includes Tyr^{726} and K^{719} [these residues are in the red regions in panel a], and the interactions at the F^7 subsite with residues Met^{339}, Lys^{340}, and Trp^{728} in panel a, which are absent in panel b.

the clear homology between the four C-terminal residues of P7 (-D^4ADF^7) and the four C-terminal residues of eR2 (-N^4FQL^7) vs the lack of homology between the N-terminal three residues of P7 (F^1TL^3-) and the 5th−7th residues from the C-terminus of eR2 (D^1LS^3-).

(a) Bound P7. The model of bound P7 (Figure 2a), constructed as described (see Experimental Section), contains extensive areas of interaction between both the N- and C-terminal Phes of the peptide and mR1,

consistent with the structure−function results summarized in Table 2. Two aromatic residues within the F^7 subsite, Trp^{728} and Phe^{725}, form edge-to-face interactions with F^7. Trp^{728} is one of the covariant cluster of residues discussed above, and Phe^{725} is strongly conserved when both the N- and C-termini of the R2 C-terminal peptide are Phe (Table 1). F^7 also packs with the side chains of Met^{339}, another of the covariant residues, and with Glu^{343}.

F^1 also shows strong interactions at the F^1 subsite, including favorable edge-to-face interactions with Tyr^{717} as well as hydrophobic packing with Glu^{387} and Phe^{725}. L^3, which is constrained to interact with F^1 by trNOE results, interacts with Asn^{345} as its primary protein contact, as well as with Glu^{343}. The importance of these interactions is shown by the 20-fold drop in affinity on substituting L^3 with Ala.[7] In contrast to F^7, the F^1 and L^3 interactions with mR1 occur along the surface of the protein and do not localize to a pocket. This is consistent with the observed lower stringency for binding at the F^1 subsite than at the F^7 subsite. The existence and properties of the F^1 subsite offer attractive rationales both for the higher affinity of P7 for mR1 vs the eR2 C-terminal octamer for eR1, since no interactions comparable to the F^1 subsite are seen between eR1 and the corresponding D^1LS^3 residues in the eR2 C-terminus, and for the promising binding of the simple molecules FmocPhe and FmocLeu (Table 2), each of which could bind to this subsite via the Fmoc group.

The interactions made by the three carboxylates in the C-terminal half of P7 are also of interest. The C-terminal carboxylate forms a salt bridge with Lys^{340}, which is highly conserved in eucaryotic and some viral R1s (Table 1), whereas D^6 salt bridges with the even more highly conserved Lys^{729}. This scheme differs from that seen in the *E. coli* structure, in which Lys^{729} forms the salt bridge with the C-terminus of the *E. coli* peptide, which, unlike P7, does not have a free carboxylate in the penultimate position. The C-terminus-Lys^{340} salt bridge appears critical for the mR1.P7 interaction, given the low binding activity of the C-terminal amide peptide **14**. By contrast, the D^6-Lys^{729} salt bridge adds little to the energetics of P7 interaction with mR1, since Ala substitution at position 6 results in little loss of affinity.[20] The third carboxylate, D^4, shows no interactions with mR1 but does hydrogen bond through its side chain to the amide of L^3. This interaction is observed in the trNOE structure of P7 and may be crucial to holding the peptide in a reverse turn conformation, given the 30-fold loss in affinity on substituting D^4 with Ala.[20]

Finally, the model shows relatively few contacts between mR1 and either residues T^2 and A^5 or the acetyl group. This is in accord with the general insensitivity of binding affinity to substitution at the 2,5[20] and N-acyl positions (Table 2).

(b) Bound cycP7. The model of bound cycP7 (Figure 2b) shows interesting similarities and differences vis-à-vis bound P7. Both molecules share common interactions at the F^1 subsite, and for both the D^6 side chain makes strong hydrogen bonds with Lys^{729}. In addition, residues E^2 and K^5 show no interaction with mR1, paralleling the lack of interaction with mR1 of P7 residues T^2 and A^5. There are, however, several important differences. Most importantly, cycP7 shows an increased interaction at the F^1 subsite at the expense of a much reduced interaction at the F^7 subsite. This difference results from the C-terminal Phe folding inward, packing with L^3, in a manner that precludes its being able to extend into the F^7 subsite. In so doing it makes a strong interaction with Tyr^{726} which now also interacts with L^3, effectively extending the F^1 subsite. Other differences at the F^1 subsite vs bound P7 include stronger interactions of F^1 with Phe^{725} and Glu^{343} and of the acetyl group with several residues, especially the Gln^{396} side chain, and a weaker L^3 interaction with Glu^{343}. A second significant difference concerns D^4, which salt bridges with Lys^{719}, whereas in bound P7 it interacts with the P7 backbone only.

The inward folding of the C-terminal Phe residue of the cyclic peptide may help explain the surprisingly small decrease in relative binding affinity (9-fold) of peptide (**15**), in which the F^7 residue is substituted with D-Phe. Naively, one would expect this substitution to completely disrupt binding at the F^7 subsite, with an accompanying large loss in binding affinity. We suspect that AcFTLDAD(D-Phe) may adopt a conformation similar to that of cycP7, in which the D-Phe side chain folds back into the peptide itself, reinforcing interaction with the F^1 subsite, though not to the same extent as the L-Phe side chain in cycP7.

Conclusions Going Forward. Why does cycP7 bind 2.5 times more tightly to mR1 than does P7,[24] despite having lost the energetically favorable interaction with the F^7 subsite? It is reasonable to assume that the answer lies in the differences noted above. Our working hypothesis is that expansion of the interaction at the F^1 subsite in cycP7 compensates for loss of F^7 interaction with the F^7 subsite, since the salt bridges seen in our models are solvent exposed and are not expected to make major contributions to binding stability. The importance of the F^1 subsite is also suggested by our finding that FmocPhe and FmocLeu show reasonably tight binding to mR1 (Table 2). Modeling studies on FmocPhe and FmocLeu in aqueous solution show that in both molecules the fluorene packs very close to the phenyl or the isobutyl side chain. Docking these conformations into the model of mR1 (not shown) demonstrates that the fluorene group binds at the F^1 subsite, occupying the binding region of F^1 and L^3 in P7. The F^7 subsite is simply too small to accommodate either molecule. It follows from these considerations that very high affinity ligands for mR1 could be developed that, while maintaining an expanded contact with the F^1 subsite, are also able to make strong contacts with the F^7 subsite. The design, synthesis, and testing of such molecules is underway.

III. Chemistry

Libraries II and III were synthesized by solid phase peptide synthesis, using standard reagents and procedures as outlined in the Experimental Section. Library I was generated by solution phase coupling of C-terminally protected Phe derivatives with the hexamer, fully protected except for the C-terminus. Phe derivatives that could be purchased with a free N-terminus and protection at the C-terminus were coupled directly. However, most Phe derivatives were only commercially

available as the N-terminally protected residues. Such derivatives were reacted with *tert*-butyl trichloroacetimidate to protect the C-terminus, followed by N-terminus deprotection. Reactions for library I were typically on the scale of 5 μmol. All peptides were purified to homogeneity by HPLC and gave molecular ions in the mass spectrum consistent with their molecular weights, with one exception (see below). The parent peptide (P7, AcFTLDADF) synthesized using this coupling procedure had a binding affinity for mR1, as measured by the binding assay, that was identical to that of P7 synthesized earlier by standard automated solid phase synthesis,[20] providing strong evidence for the lack of racemization during library I generation.

The mass spectrum of AcFTLDADPhe(*o*-OH) **16** gave a molecular ion 18 mass units less than expected. We attribute this to condensation of the *o*-hydroxy group with the C-terminus, forming a lactone which is a 3-subsituted-3,4-dihydrocoumarin. Such lactone formation is favored under the acidic conditions employed for deprotection. However, known pH effects on both the rate and equilibrium position of 3,4-dihydrocoumarin ring opening[37,38] strongly suggest that the ring-opened form dominates under our binding assay conditions, at pH 8.5.

IV. Conclusions

We report the use of a new, more efficient and less expensive assay to directly measure the binding of a peptide ligand to the R2 C-terminal peptide binding site of mR1, demonstrate that such binding parallels peptide ligand inhibitory effects on mRR activity, and determine binding affinities to mR1 of peptides formed by substitution at the N-terminal, F^1, and F^7 positions of the R2 C-terminal peptide N-Ac-FTLDADF (denoted P7), as well as of N-protected Phe and Leu. The results of these studies, and of earlier studies of P7 substitutions, are consistent with a structural model of the mR1.P7 complex in which the dominant interactions of P7 occur at two distinct mR1 loci, the F^1 and F^7 subsites. The model is created using QUANTA 97 and is based on (a) the crystal structure of the R1 from *E. coli* (eR1) complexed with the C-terminal peptide from *E. coli* R2 (eR2), (b) the aligned sequences of mR1 and eR1, (c) the trNOE-derived structure of P7 bound to mR1. Comparison of this model with similar models constructed for the mR1 complex with both a high affinity cyclic peptide analogue of P7 and with FmocPhe indicates that increased interaction at the F^1 subsite can offset loss of F^7 subsite interaction, and it suggests strategies for the design of new, higher affinity inhibitors of mRR.

V. Experimental Section

Materials. AcFT(tBu)LD(OtBu)AD(OtBu) was purchased from SynPep corporation (Dublin, CA). FTLDADF either was purchased from Research Genetics (Huntsville, AL), or was prepared by Dr. Alison Fisher, as described.[20] AcFTLDADF was also prepared by Dr. Alison Fisher, as described.[20] An ASI431A peptide synthesizer (Applied Biosystem Inc.) was used to synthesize peptide precursors, Fmoc-FT(tBu)LD-(OtBu)AD(OtBu)F-Wang resin for library II and Fmoc-T(tBu)-LD(OtBu)AD(OtBu)F-Wang resin for library III, following the operation procedure in the manual. Boc-2-fluoro-L-Phe, Boc-2-chloro-L-Phe, Boc-2-pyridyl-L-alanine, and Boc-3-pyridyl-L-alanine were purchased from American Peptide Company (Sunnyvale, CA). H-D-Phe-OtBu·HCl, H-His(Trt)-OtBu·HCl, and Boc-pentafluoro-L-Phe were purchased from ChemImpex International (Wood Dale, IL). Boc-Phe was purchased from Sigma. Fmoc-2-hydroxy-L-Phe, Fmoc-2-methoxy-L-Phe, Fmoc-3-hydroxy-L-Phe, Fmoc-3-methoxy-L-Phe, Fmoc-4-methyl-L-Phe, and Fmoc-L-cyclohexylalanine were a gift from RSP amino acids (Worcester, MA). Fmoc-*p*-Nitro-L-Phe, Fmoc-*p*-Amino-(Boc)-L-Phe, Fmoc-L-Tyr(tBu), H-L-Phe-OtBu·HCl, H-L-Trp-OtBu·HCl, H-L-Phg-OtBu·HCl, H-L-Phe-NH_2, and all other Fmoc amino acids were purchased from Bachem Bioscience (King of Prussia, PA). FmocPhe-Wang resin, HBTU, and HOBT were purchased from Nova Biochem (La Jolla, CA). The solvents for peptide synthesis were purchased from Fisher Scientific (Pittsburgh, PA). MicroSpin columns, activated CH Sepharose 4B, and 8-^{3}H-GDP were purchased from Amersham Pharmacia Biotech (Piscataway, NJ). Phenyl Boronate Agarose gel (PBA-60) was purchased from Millipore (Bedford, MA). All other chemicals were from Aldrich or Sigma (St. Louis, MO).

The plasmid pET-M2 (pET3a-R2) encoding the mouse R2 subunit was a gift from Dr. Lars Thelander[39] and was grown in BL21(DE3) cells. mR2 was purified by a published method,[40] with slight modification as outlined in the thesis of Christian Hamann.[41] The gene encoding the large (R1) subunit of mouse ribonucleotide reductase was a gift from Dr. Ingrid Caras (Genentech).[42] mR1 was expressed and purified as described previously.[43]

New R1-Peptide Binding Assay. The preparation of FTLDADF-Sepharose was described previously.[19] Briefly, CH Sepharose 4B (10 g) is suspended in 50 mL of 1 mM HCl, subsequently washed on a Buchner funnel with 1.95 L of 1 mM HCl, and dried under suction. The filter cake is added to 50 mL of 0.1 M $NaHCO_3$ containing 15 mg of FTLDADF. The reaction mixture is agitated on a shaker table at room temperature, and A_{260} is monitored to follow release of the imidazole group from the resin. Once the A_{260} levels off ($\sim$4 h), the reaction is quenched by adding 50 mL of 2 M glycine, and agitated for 1 h. FTLDADF-Sepharose is collected on a fritted funnel (coarse), washed with 500 mL of 50 mM Tris-Cl, pH 7.6, and suspended and stored in 60 μM NaN_3.

For the R1-peptide binding assay wet column material ($\sim$ 75 μL) is aliquotted into MicroSpin columns, followed by equilibration with 2 $\times$ 75 μL of buffer A (50 mM Tris, pH 8.5, 10 mM DTT, 100 μM dTTP). Added DTT keeps R1 in reduced form, preventing aggregation due to intermolecular disulfide formation. Added dTTP (100 μM) ensures all R1 is maintained in the dimeric state. The assay works best when the elution of mR1 is minimal in the absence of added inhibitor and maximal in the presence of a potent inhibitor, as tested with 100 μM P7. In maintaining this balance, it is usually desirable to mix FTLDADF-Sepharose with underivatized Sepharose 4B-Cl. A typical mixing ratio is 60:40: i.e., a column would have 45 μL of FTLDADF-Sepharose prepared as above and 30 μL of Sepharose 4B-Cl. In addition, pH 8.5 is superior to pH 7.5. Complete elution of R1 corresponded to 70 $\pm$ 10% of that applied.

After each addition of buffer (or later of wash or sample), columns are spun for 1 min at 735*g* in a Heraeus pico Biofuge (VWR). Premixed samples of mR1 (4.4 μM) and inhibitor (typically 100 μM) in buffer A (50 μL total) are loaded onto individual columns and allowed to sit for 30 min. The columns are then centrifuged, and the eluate is collected in an eppendorf tube followed by a 50 μL wash with buffer A, collected in the same tube. The column material is regenerated by washing with 2 $\times$ 150 μL of 6 M guanidinium chloride, followed by 2 $\times$ 150 μL wash and subsequent storage in 60 μM NaN_3. Eluate from each sample is analyzed for R1 content by Bradford assay.[44] All samples are run in duplicate. Table 4 shows sample data from our column assay, demonstrating an increase in protein elution upon introduction of higher concentrations of inhibitor.

Calculating K_ds Using the R1-Peptide Binding Assay. The amount of eluted mR1 in the presence of a ligand competing with Sepharose-FTLDADF for mR1 binding provides a measure of the affinity of mR1 for the free ligand. To convert this information into a quantitative estimate of ligand

Table 4. Sample Data from the New R1-Peptide Binding Assay

	R1 eluted (μg)	
[inhibitor] (μM)	AcFTLDADF	Fmoc Phe
10	1.3	
30	2.1	0.9
100	3.8	1.3
300	7.7	2.7
1000	10.9	8.7

binding relative to that of the standard inhibitor, P7, each assay is standardized by measuring mR1 elution both with no inhibitor present and in the presence of P7. The following equations are pertinent, where K_a is the dissociation constant of ligand L_a, K_{P7} is the dissociation constant of P7, $[L_c]_{eff}$ is the effective concentration of column-bound FTLDADF, K_c is the dissociation constant for the binding of the column-bound FTLDADF to mR1, $[mR1]_t$ is the total mR1 concentration in the column prior to centrifugation, and $[mR1]_e$ is the measured concentration of eluted mR1 protein following centrifugation.

$$K_c = [mR1][L_c]_{eff}/[mR1L_c] \quad (1)$$

$$K_a = [mR1][L_a]/[mR1L_a] \quad (2)$$

$$[mR1]_t = [mR1] + [mR1L_c] + [mR1L_a] \quad (3)$$

$$[mR1]_e = [mR1] + [mR1L_a] \quad (4)$$

Combining eqs 1, 2, and 3 yields

$$[mR1]_t = [mR1](\alpha + \beta) \quad (5)$$

$$\text{where } \beta = 1 + ([L_a]/K_a)$$

$$\text{and } \alpha = [L_c]_{eff}/K_c$$

Combining eqs 2 and 4 yields

$$[mR1] = [mR1]_e/\beta \quad (6)$$

Combining eqs 5 and 6 and rearranging yields

$$\alpha = \beta\,\{([mR1]_t/[mR1]_e) - 1\} \quad (7)$$

Determination of $[mR1]_e$ in the presence and absence of an inhibitor L_a obviates the need to evaluate α explicitly, since

$$\alpha = \{1 + [L_a]/K_a\}\{[mR1]_t/[mR1]_{e,a} - 1\} = \{[mR1]_t/[mR1]_{e,0} - 1\} \quad (8)$$

where $[mR1]_{e,a}$ is the eluted protein in the presence of an inhibitor L_a, and $[mR1]_{e,0}$ is the eluted protein with no inhibitor present. Solving for K_a:

$$K_a = [L_a][mR1]_{e,0}\{[mR1]_t - [mR1]_{e,a}\}/[mR1]_t\{[mR1]_{e,a} - [mR1]_{e,0}\} \quad (9)$$

In the work presented in this paper, free $[L_a]$ is well approximated by total $[L_a]$.

Although K_d values calculated directly from eq 9 are subject to considerable variation [e.g., the value found for P7 was 9 ± 5 μM (12 determinations)], the dissociation constant for any inhibitor L_a relative to the P7 standard, calculated from eq 10, is quite reproducible. Such relative values are reported in Table 2.

$$K_a/K_{P7} = [L_a]\{[mR1]_t - [mR1]_{e,a}\}\{[mR1]_{e,P7} - [mR1]_{e,0}\}/[L_{P7}]\{[mR1]_{e,a} - [mR1]_{e,0}\}\{[mR1]_t - [mR1]_{e,P7}\} \quad (10)$$

where $[mR1]_{e,P7}$ is the protein eluted in the presence of P7.

The precision with which relative *K*s can be determined from eq 10 is limited by the term $\{[mR1]_{e,a} - [mR1]_{e,0}\}$ as $[mR1]_{e,a}$ approaches $[mR1]_{e,0}$ for very weak inhibitors. Thus, values above 30 have large average deviations and are considered unreliable.

In Vitro Ribonucleotide Reductase Activity Assay. Ribonucleotide reductase activity was assayed at 37 °C by monitoring the conversion of [^{3}H]-GDP to [^{3}H]-dGDP essentially as previously described.[19,20] In a volume of 70 μL, each assay contained 60 mM HEPES, pH 7.6, 10 mM $MgCl_2$, 8.75 mM NaF, 25 mM DTT, 300 μM dTTP, 50 μM $FeCl_3$, 100 μM [8-^{3}H]-GDP, 2 μg of R1, 4 μg of R2, and varying amounts of peptide inhibitors. Reactions were initiated with the radiolabeled substrate and quenched by immersion in a boiling water bath for 5 min. Tritiated samples were frozen and lyophilized to dryness to reduce backgrounds. Lyophilized samples were reconstituted in 1 mL of 50 mM Tris-HCl, pH 8.5, with 100 mM $Mg(OAc)_2$ (buffer B) and centrifuged at 6000*g* for 10 min in a microfuge to remove denatured protein. Reconstituted samples were loaded onto phenylboronate-agarose columns (2 mL bed volume), preequilibrated with 10 mL of buffer B. Deoxyribonucleoside diphosphates elute in 8 mL of buffer B. Unreacted ribonucleoside diphosphate substrates were recovered and columns were regenerated by treatment with 10 mL of 50 mM sodium citrate, pH 5.9. Recovery typically ranged between 75% and 100% of label. Radioactivity in aliquots of both buffer B and citrate fractions was measured by liquid scintillation counting.

Peptide stocks were made by adding base (either 0.1 M NaOH or saturated $NaHCO_3$) to a suspension of lyophilized peptide in water until full solution was obtained (final pH 8.0−8.5). The concentrations of the peptide stocks were determined from analytical HPLC injections by comparing the area under the absorption peak (215 nm) with a standard sample of AcFTLDADF. The validity of this approach was confirmed for several peptides using extinction coefficients for either phenylalanine (258 nm) or for the side chains of the phenylalanine analogues.

C-Terminal Protection of N-Terminally Protected Phenylalanine Analogues. Reactions were performed typically on a scale of 100 μmol, following a published procedure.[45] Typically, 200 μL of 1 M *tert*-butyl-2,2,2-trichloroacetimidate in cyclohexane was added to 1 mL of 0.1 M phenylalanine analogue in DCM, and the reaction was either maintained at room temperature for ~2 days or refluxed for 3−5 h. Reactions were stopped by evaporating solvent under reduced pressure when no further consumption of starting material was noted by TLC (silica, 0.5% MeOH in $CHCl_3$), using ninhydrin staining. Fully protected phenylalanine analogues were purified by silica gel flash chromatography. Each demonstrated an M + H or M + Na peak in electrospray mass spectrometry (Micromass platform mass spectrometer, Manchester, U.K.) consistent with its molecular mass.

N-Terminal Deprotection of Phenylalanine Analogues. Reactions were performed typically on a scale of 10−20 μmol. FmocPhe derivatives in DCM (2 volumes, 0.1 M) were deprotected by addition of one volume of diethylamine. Boc-Phe derivatives in ethyl acetate (3 volumes, 0.27 M) were deprotected as described,[46] with slight modification, by reaction with a 5-fold excess of 4 M HCl in dry dioxane (1 volume). In both cases, reactions were monitored by TLC as above and were complete in 1−2 h at room temperature. No purification of these materials was performed prior to the coupling reaction described below.

Synthesis of Library 1: AcFTLDAD*X*. Reactions were performed, under argon, with either one phenylalanine analogue or with two phenylalanine analogues simultaneously. Typically, 4.5 mg (5 μmol, 1 equiv) of AcFT(tBu)LD(OtBu)-AD(OtBu), 1.4 mg of HOBt (10 μmol, 2 equiv), and 0.7 μL of triethylamine (TEA) (5 μmol, 1 equiv) were dissolved in a minimum amount of DCM at 4 °C. EDC (1.5 mg, 7.5 μmol, 1.5 equiv) and additional equivalent(s) of TEA, if needed to neutralize hydrochloride salts, were added to the C-terminally protected amino acid (2 equiv total). Reaction was initiated

by addition of the peptide solution to the solution of EDC and amino acid(s). Occasionally, a small volume of DMF was added to increase amino acid solubility. The reaction was started on ice and allowed to warm to room temperature overnight, checked for completion by TLC on silica (9 mL:1 mL:1 drop DCM/MeOH/AcOH), and evaporated to an oil under reduced pressure. The crude oil was dissolved in 30 mL of ethyl acetate, washed two times with 10 mL of 1 M HCl, once with 10 mL of saturated $NaHCO_3$, and once with 15 mL of brine. The organic layer was dried over $MgSO_4$ and evaporated to dryness under reduced pressure. The protected 7-mer was deprotected in 95% TFA using anisole (50-fold molar excess) as a scavenger. For AcFTLDADW, deprotection was carried out in 50% TFA, 3.1% ethanedithiol, and 2% water in DCM. The peptide was allowed to sit for 1−2 h at room temperature, and the TFA was evaporated under reduced pressure. The crude peptide then was dissolved in 1:1 acetonitrile/water with 0.1% TFA and lyophilized overnight to yield a dry powder.

Synthesis of Library II. Ac*X*TLDADF. Fmoc-T(tBu)LD-(OtBU)AD(OtBu)F-Wang resin (22 mg, 0.01 mmol of peptide) was treated with 20% piperidine in NMP (10 mL/1 g resin) for 30 min at room temperature to remove the Fmoc-group. The resin was removed by filtration, and washed with NMP and DCM (3 mL each time, 3 times each solvent), before being reacted for 2 h at room temperature with a solution of Fmoc-amino acid (0.10 mmol) in 5 mL NMP containing HBTU (15.2 mg, 0.04 mmol), HOBT (6.1 mg, 0.04 mmol), and DIEA (10 μL, 0.05 mmol). Completion of the reaction was verified by Kaiser test.[47] N-Terminal acetylation with acetic anhydride was carried out as described below. Peptides were deprotected and cleaved from the resin by treatment with 95% TFA (10 mL/1 g resin) for 90 min at room temperature[20] and precipitated and washed exhaustively with anhydrous diethyl ether.

Synthesis of Library III. *X*FTLDADF. Fmoc-FT(tBu)LD-(OtBu)AD(OtBu)F-Wang resin was deblocked with 20% piperidine in NMP as described above. Three methods of N-terminal acylation were employed following deblocking, all using 0.01 mmol of peptide bound to resin. Method 1: Resin was reacted for 1 h at room temperature with 2 mmol of anhydride (acetic, propionic, butyric, or benzoic) in 4 mL of NMP containing DIEA (0.09 mL, 0.5 mmol) and HOBT (9.2 mg, 0.06 mmol). Method 2: Resin was reacted for 2 h at room temperature with 0.10 mmol of carboxylic acid (phenylacetic, *p*-methoxylphenylacetic, or *p*-nitrophenylacetic) in 5 mL of NMP containing HBTU (15.2 mg, 0.04 mmol), HOBT (6.1 mg, 0.04 mmol), DIEA (10 μL, 0.05 mmol). Method 3: HCO-FTLDADF was synthesized using the mixed anhydride procedure.[48] At 0 °C, 0.5 mL of acetic anhydride was added dropwise to 1 mL of formic acid, and the mixture was stirred for 10 min. The reaction mixture was then stirred at room temperature for 1 h, diluted by addition of 3 mL of DCM, and added into the reaction vessel containing peptide. The reaction vessel was shaken for 2 h at room temperature. Completion of all capping reactions was verified by Kaiser test. Peptides were deprotected and cleaved from the resin by treatment with 95% TFA (10 mL/1 g resin) for 90 min at room temperature, and precipitated and washed exhaustively with anhydrous diethyl ether.

Purification and Characterization of Peptides. All peptides were purified by HPLC (Synchropak C_{18} column, Micra Scientific Inc., or Microsorb-MV C-18, (Keystone Scientific, Bellefonte, PA) with a Perkin-Elmer Series 4 Chromatograph HPLC) using a linear gradient of acetonitrile in 0.1% TFA. Collected fractions were lyophilized and reinjected to assess purity and determine peptide stock concentration. Each peptide had either or both M + H and M + Na peaks in its mass spectrum consistent with its molecular mass, and each was >95% pure, except in two cases. AcFTLDAD(*o*OH-Phe) **14** was only 85% pure. AcFTLDAD(*o*OMe-Phe **18**)/AcFTLDAD-(*p*NO_2-Phe) **19** were prepared in the same reaction and were co-purified and assayed for mR1 binding as a mixture having a 53:47 composition, as estimated by mass spectrometric analysis. Both samples had very low affinity for mR1.

Molecular Modeling. Models for the solution conformations of FmocPhe and Fmoc Leu were created using the GB/SA continuum model in MacroModel (Schrödinger Inc., Jersey City, NJ). Structural models of mR1 complexes were created using QUANTA 97 (Molecular Simulations, Inc., Burlington, MA) and the crystal structure of *E. coli* R1 (RCSB Protein Data Bank code 1RLR).[26,49] This structure includes a bound decameric peptide (DIDDLSNFQL) corresponding to the C-terminal residues of the *E. coli* R2 protein. We used this decameric peptide, residues in eR1 within 7 Å of the decameric peptide, and the sequence alignment of mR1 and eR1 from CLUSTALW (Figure 1) to build a model of mR1. Residue side chains in eR1 were manually changed to the corresponding side chains in mR1 at positions in which their sequences differed, and the decameric peptide was reduced in length to the acetylated heptameric peptide. Distance constraints from the trNOE experiments for P7 and cycP7, numbering 74 and 69, respectively, were imposed on the peptides, and positional constraints were imposed on all backbone atoms of the mR1 model. Exhaustive energy minimization was then performed using the adapted basis Newton−Raphson algorithm, a radial dielectric function, and the Charmm force field implemented within QUANTA 97. The model for bound P7 (Figure 2a) exhibits 18 lower bound violations vis-à-vis the trNOE constraints, which averaged 0.2 Å each (0.5 Å being the largest deviation), and two upper bound violations of 0.1 and 0.9 Å. The corresponding values for the model of bound cycP7 (Figure 2b) are 12 lower bound violations which averaged 0.2 Å each (0.8 Å being the largest deviation), and 4 upper bound violations totaling only 0.05 Å. An especially important constraint for the models of both bound P7 and bound cycP7, was that between the side chains of F^1 and L^3. Two other constraints important for the P7 model were those between the side chains of A^5 and F^7, as well as the T^2-A^5 constraint, which helps define the turn.

Abbreviations. Abbreviations for common amino acids are in accordance with the recommendations of IUPAC. Additional abbreviations: Boc, *tert*-butoxycarbonyl; cycP7, AcFcyc[ELDK]-DF; DCM, dichloromethane; DIEA, *N*,*N*-diisopropylethylamine; DMF, *N*,*N*-dimethyl fomamide; EDC, 1-ethyl-3,3-dimethylaminopropylcarbodiimide; DTT, dithiothreitol; eRR, *E. coli* RR; Fmoc, fluorenylmethoxycarbonyl; HBTU, 2-(1*H*-benzotriazol-1-yl)-1,1,3,3-tetramethyluronium hexafluorophosphate; HEPES, *N*-2-hydroxyethylpiperazine-*N*′-2-ethanesulfonic acid; HOBT, *N*-hydroxybenzotriazole; mRR, mouse RR; NMP, *N*-methylpyrrolidone; P7, AcFTLDADF; RR, ribonucleotide reductase; TEA, triethylamine; TFA, trifluoroacetic acid; Tris-Cl, tris(hydroxymethyl)aminomethane hydrochloride; trNOE, transfer nuclear Overhauser effect.

Acknowledgment. This work was supported by NIH Grant CA58567 to B.S.C. B.A.P. was also supported by NIH Training Grant T32 GM 07229. We thank Dr. Alison Fisher for providing P7, Dr. Shri Nair for providing the inhibition results with peptide 33, Dr. Jian Liu for modeling the conformations of FmocPhe and FmocLeu in solution, and Professor Dale Mierke for helpful discussions.

References

(1) Jordan, A.; Reichard, P. Ribonucleotide reductases. *Annu. Rev. Biochem.* **1998**, *67*, 71−98.
(2) Stubbe, J.; van der Donk, W. A. Ribonucleotide reductases: radical enzymes with suicidal tendencies. *Chem. Biol.* **1995**, *2*, 793−801.
(3) Szekeres, T.; Fritzer-Szekeres, M.; Elford, H. L. The enzyme ribonucleotide reductase: target for antitumor and anti-HIV therapy. *Crit. Rev. Clin. Lab. Sci.* **1997**, *34*, 503−28.
(4) Robins, M. J. Mechanism-based inhibition of ribonucleotide reductases: new mechanistic consideration and promising biological applications. *Nucleosides Nucleotides* **1999**, *18*, 779−93.
(5) Hui, Y. F.; Reitz, J. Gemcitabine: a cytidine analogue active against solid tumors. *Am. J. Health Syst. Pharm.* **1997**, *54*, 162−70.
(6) Stevens, M. R. Hydroxyurea: an overview. *J. Biol. Regul. Homeost. Agents* **1999**, *13* (3), 172−5.

(7) Romanelli, F.; Pomeroy, C.; Smith, K. M. Hydroxyurea to inhibit human immunodeficiency virus-1 replication. *Pharmacotherapy* **1999**, *19* (2), 196−204.
(8) Hainsworth, J. D.; Burris, H. A., III; Litchy, S.; Erland, J. B.; Hon, J. K.; Brierre, J. E.; Greco, F. A. Gemcitabine and vinorelbine in the second-line treatment of nonsmall cell lung carcinoma patients: a minnie pearl cancer research network phase II trial. *Cancer* **2000**, *88* (6), 1353−8.
(9) Berlin, J. D.; Adak, S.; Vaughn, D. J.; Flinker, D.; Blaszkowsky, L.; Harris, J. E.; Benson, A. B., III A phase II study of gemcitabine and 5-fluorouracil in metastatic pancreatic cancer: an Eastern Cooperative Oncology Group Study (E3296). *Oncology* **2000**, *58* (3), 215−8.
(10) Lorusso, V.; Manzione, L.; De Vita, F.; Antimi, M.; Selvaggi, F. P.; De Lena, M. Gemcitabine plus cisplatin for advanced transitional cell carcinoma of the urinary tract: a phase II multicenter trial. *J. Urol.* **2000**, *164* (1), 53−6.
(11) Matano, E.; Tagliaferri, P.; Libroia, A.; Damiano, V.; Fabbrocini, A.; De Lorenzo, S.; Bianco, A. R. Gemcitabine combined with continuous infusion 5-fluorouracil in advanced and symptomatic pancreatic cancer: a clinical benefit-oriented phase II study. *Br. J. Cancer* **2000**, *82* (11) 1772−5.
(12) Nagourney, R. A.; Link, J. S.; Blitzer, J. B.; Forsthoff, C.; Evans, S. S. Gemcitabine plus cisplatin repeating doublet therapy in previously treated, relapsed breast cancer patients. *J. Clin. Oncol.* **2000**, *18* (11), 2245−9.
(13) Adjei, A. A.; Erlichman, C.; Sloan, J. A.; Reid, J. M.; Pitot, H. C.; Goldberg, R. M.; Peethambaram, P.; Atherton, P.; Hanson, L. J.; Alberts, S. R.; Jett, J. Phase I and pharmacologic study of sequences of gemcitabine and the multitargeted antifolate agent in patients with advanced solid tumors. *J. Clin. Oncol.* **2000**, *18* (8), 1748−57.
(14) Linskens, R. K.; Golding, R. P.; van Groeningen, C. J.; Giaccone, G. Severe acute lung injury induced by gemcitabine. *Neth. J. Med.* **2000**, *56* (6), 232−5.
(15) Santini, D.; Tonini, G.; Abbate, A.; Di Cosimo, S.; Gravante, G.; Vincenzi, B.; Campisi, C.; Patti, G.; Di Sciascio, G. Gemcitabine-induced atrial fibrillation: a hitherto unreported manifestation of drug toxicity. *Ann. Oncol.* **2000**, *11* (4), 479−81.
(16) Banach, M. J.; Williams, G. A. Purtscher retinopathy and necrotizing vasculitis with gemcitabine therapy. *Arch. Ophthalmol.* **2000**, *118* (5), 726−7.
(17) Mansson, E.; Spasokoukotskaja, T.; Sallstrom, J.; Eriksson, S.; Albertioni, F. Molecular and biochemical mechanisms of fludarabine and cladribine resistance in a human promyelocytic cell line. *Cancer Res.* **1999**, *59*, 5956−63.
(18) Duan, J.; Liuzzi, M.; Paris, W.; Lambert, M.; Lawetz, C.; Moss, N.; Jaramillo, J.; Gauthier, J.; Deziel, R.; Cordingley, M. G. Antiviral activity of a selective ribonucleotide reductase inhibitor against acyclovir-resistant herpes simplex virus type 1 in vivo. *Antimicrob Agents Chemother.* **1998**, *42*, 1629−35.
(19) Yang, F.-D.; Spanevello, R. A.; Celiker, I.; Hirschman, R.; Rubin, H.; Cooperman, B. S. The carboxyl terminus heptapeptide of the R2 subunit of mammalian ribonucleotide reductase inhibits enzyme activity and can be used to purify the R1 subunit. *FEBS Lett.* **1990**, *272*, 61−4.
(20) Fisher, A.; Yang, F.-D.; Rubin, H.; Cooperman, B. S. R2 C-terminal peptide inhibition of mammalian and yeast ribonucleotide reductase. *J. Med. Chem.* **1993**, *36*, 3859−62.
(21) Fisher, A.; Laub, P. B.; Cooperman, B. S. NMR structure of an inhibitory R2 C-terminal peptide bound to mouse ribonucleotide reductase R1 subunit. *Nature Struct. Biol.* **1995**, *2*, 951−5.
(22) Laub, P. B.; Fisher, A.; Cooperman, B. S. Small C-terminal Inhibitory Peptide of Mouse Ribonucleotide Reductase As Bound To The Large Subunit. *Nmr, 26 Structures, Protein Databank* Id: 1AFT, MMDB Id: 5993 **1997**.
(23) Pellegrini, M.; Liehr, S.; Fisher, A. L.; Laub, P. B.; Cooperman, B. S.; Mierke, D. F. Structure-Based Optimization of Peptide Inhibitors of Mammalian Ribonucleotide Reductase. *Biochemistry* **2000**, *39*, 12210−5.
(24) Liehr, S.; Barbosa, J.; Smith, A. B., III; Cooperman, B. S. Synthesis and biological activity of cyclic peptide inhibitors of ribonucleotide reductase. *Org. Lett.* **1999**, *1*, 1201−4.
(25) Smith, A. B., III; Sasho, S.; Barwis, B. A.; Sprengeler, P.; Barbosa, J.; Hirschmann, R.; Cooperman, B. S. Design and synthesis of a tetrahydropyran-based inhibitor of mammalian ribonucleotide reductase. *Bioorg. Med. Chem. Lett.* **1998**, *8*, 3133−6.
(26) Uhlin, U.; Eklund, H. Structure of ribonucleotide reductase protein R1. *Nature* **1994**, *370*, 533−9.
(27) Filler, R., Kobayashi, Y., Yagupolskii, L. M., Eds. In *Organofluorine Compounds in Medicinal Chemistry and Biomedical Applications;* Elsevier: New York, 1993; p 2.
(28) Guindon, Y.; Lavallee, P.; Sumanas, R.; Consentino, G. P. Ribonucleotide reductase inhibitors. E.P. 0 383 190 A2.
(29) Aggarwal, R. Alignment of the mouse, HSV, and malarial R1 subunit sequences of ribonucleotide reductase to the E. coli R1 crystal structure using sequence- and structure-based alignment techniques. University of Pennsylvania, Philadelphia, 1997.
(30) Sander, C.; Schneider, R. Database of homology-derived structures and the structural meaning of sequence alignment. *Proteins* **1991**, *9*, 56−68.
(31) Davis, R.; Thelander, M.; Mann, G. J.; Behraven, G.; Soucy, F.; Beaulieu, P.; Lavallée, P.; Graslund, A.; Thelander, L. Purification, characterization, and localization of subunit interaction area of recombinant mouse ribonucleotide reductase. *J. Biol. Chem.* **1994**, *269*, 23171−6.
(32) Bonneau, A. M.; Kibler, P.; White, P.; Bosquet, C.; Danserau, N.; Cordingley, M. G. Resistance of Herpes Simplex Virus Type 1 to peptidomimetic ribonucleotide reductase inhibitors: Selection and characterization of mutant isolates. *J. Virol.* **1996**, *70*, 787−93.
(33) Ekberg, M.; Sahlin, M.; Eriksson, M.; Sjöberg, B. M. Two conserved tyrosine residues in protein R1 participate in an intermolecular electron transfer in ribonucleotide reductase. *J. Biol. Chem.* **1996**, *34*, 20655−9.
(34) Grantham, R. Amino acid difference formula to help explain protein evolution. *Science* **1974**, *185*, 862−4.
(35) Hamann, C. S.; Lentainge, S.; Li, L.-S.; Salem, J. S.; Yang, F.-D.; Cooperman, B. S. Chimeric small subunit inhibitors of mammalian ribonucleotide reductase: a dual function for the R2 C-terminus? *Protein Eng.* **1998**, *11* (3), 219−24.
(36) Climent, I.; Sjöberg, B.-M.; Huang, C. Y. Carboxyl-terminal peptides as probes for *Escherichia coli* ribonucleotide reductase subunit interaction: kinetic analysis of inhibition studies. *Biochemistry* **1991**, *30*, 5164−71.
(37) Mattoo, B. N. Spectrophotometric study of the hydrolysis of coumarin and dissociation of *cis*-coumarinic acid. *Trans. Faraday Soc.* **1957**, *53*, 760−6.
(38) Bowden, K.; Hanson, M. J.; Taylor, G. R. Reactions of carbonyl compounds in basic solutions. Part 1. The alkaline ring fission of coumarins. *J. Chem. Soc.* (*B*) **1968**, *2*, 174−7.
(39) Mann, G. J.; Graslund, A.; Ochiai, E.; Ingemarson, R.; Thelander, L. Purification and characterization of recombinant mouse and herpes simplex virus ribonucleotide reductase R2 subunit. *Biochemistry* **1991**, *30*, 1939−47.
(40) Studier, F. W.; Rosenberg, A. H.; Dunn, J. J.; Dubendorff, J. W. Use of T7 RNA Polymerase to direct expression of cloned genes. *Methods Enzymol.* **1990**, *185*, 60−89.
(41) Hamann, C. S. Purification, characterization and activity of chimeric *Escherichia coli*, Mouse and Plasmodium falciparum small subunits of type 1 ribonucleotide reductase. University of Pennsylvania, Philadelphia, 1994, p 181.
(42) Caras, I. W.; Levinson, B. B.; Fabry, M.; Williams, S. R.; Martin, D. W. J. Cloned mouse ribonucleotide reductase subunit M1 cDNA reveals amino acid sequence homology with *Escherichia coli* and herpesvirus ribonucleotide reductases. *J. Biol. Chem.* **1985**, *260*, 7015−22.
(43) Salem, J. S.; Scott, C. P.; Li, L.-S.; Cooperman, B. S.; Rubin, H. High level expression of the large subunit of mouse ribonucleotide reductase in a baculovirus system. *FEBS Lett.* **1993**, *323*, 93−5.
(44) Bradford, M. M. A rapid and sensitive method for the quantitation of microgram quantities of protein utilizing the principle of protein-dye binding. *Anal. Biochem.* **1976**, *72*, 249−54.
(45) Thierry, J.; Yue, C.; Potier, P. 2-phenyl isopropyl and *tert*-Butyl trichloroacetimidates: useful reagents for ester preparation of N-Protected amino acids under neutral conditions. *Tetrahedron Lett.* **1998**, *39*, 1557−60.
(46) Gibson, F. S.; Bergmeier, S. C.; Rapoport, H. Selective removal of an N-BOC protecting group in the presence of a *tert*-butyl ester and other acid-sensitive groups. *J. Org. Chem.* **1994**, *59*, 3216−18.
(47) Kaiser, E.; Colescott, R. L.; Bossinger, C. D.; Cook, P. I. Color test for detection of free terminal amino groups in the solid-phase synthesis of peptides. *Anal. Biochem.* **1970**, *34*, 595−8.
(48) Zoete, V.; Bailly, F.; Catteau, J.-P.; Bernier, J.-L. Design, synthesis and antioxidant properties of ovothiol-derived 4-mercaptoimidazoles. *J. Chem. Soc., Perkin Trans.* **1997**, *1*, 2983−8.
(49) Hansch, C.; Leo, A. In *Substituent constants for correlation analysis in chemistry and biology*; John Wiley & Sons: New York, 1979; p 48−52.
(50) Creighton, T. E. In *Proteins: Structures and Molecular Properties,* 2nd ed.; W. H. Freeman and Co.: New York, 1993; p 154.
(51) Berman, H. M.; Westbrook, J.; Feng, Z.; Gilliland, G.; Bhat, T. N.; Weissig, H.; Shindyalov, I. N.; Bourne, P. E. The Protein Data Bank. *Nucleic Acids Res.* **2000**, *28*, 235−42.
(52) Nicholls, A.; Bharadwaj, R.; Honig, B. GRASP: graphical representation and analysis of surface properties. *Biophys. J.* **1993**, *64*, 166−70.

JM000335R